

# Can We Locate the Quench Origin with Second Sound?

Fermilab PARTI 2010 Summer Internship Report

Yu. Maximenko

*Moscow Institute of Physics and Technology*

Supervisor D.A. Sergatskov

Particle acceleration with superconducting niobium RF cavities is a prime technique in the linear electron-positron collider. Defects and impurities prevent cavities from reaching higher values of electric field, and most of the cavities quench. The location of the spot causing the cavity to quench is important because the spot should be explored for the sake of a further accelerating gradient increase in the cavity. A newly developed method of locating quenches in SRF cavities by detecting second sound waves has been gaining popularity in SRF laboratories. The technique is based on the measurements of time delays between the quench, as determined by the RF system, and the arrival of the 2nd sound wave to multiple detectors placed around the cavity in superfluid helium. Unlike multi-channel temperature mapping, this approach requires only a few sensors and simple readout electronics; it can be used with SRF cavities of almost arbitrary shape. One of its drawbacks is that being an indirect method it requires one to solve the inverse problem of finding the location of the quench. We tried to solve this inverse problem by using a parametric forward model. By analyzing the data we found that the approximation where the 2nd-sound emitter is a near-singular source does not describe the physical system well enough. Analysis of the quench process can be helpful in creating a more adequate model. We present here our current algorithm solving the inverse problem and discuss the experimental results.

TD-10-024

# 1 Introduction

Modern particle physics made much account of linear collider experiments. Superconducting radio frequency (SRF) cavities (Fig.1) are the prime technique for particle acceleration in linear colliders [1]. Maximum possible field accelerating gradient moves forward maximum particle energy with the same costs. The main problem with SRF cavities is that none of them are able to reach the critical magnetic field for the material they are made of. Most of the cavities quench, and it happens to all appearance due to the defects and impurities. To increase the accelerating gradient value in the SRF cavities we should understand the quench process nature. The first step is to establish a procedure for locating the quench origin on the cavity surface. In the present paper we will discuss the problem solving technique using the second sound.



Figure 1: 1.3 GHz SRF TESLA cavity

## 2 Problem definition

One need to locate the quench source on the cavity surface in order to find out why cavities cannot reach the theoretically predicted field limit. The quench arises from the spot on the inner surface of the cavity due to some defects or impurities. Niobium becomes normal conductor locally and starts to heat up. The heat propagates from this point through the niobium to the external surface and forms there a hot spot. The temperature of this spot can reach 100K [2] [3].

To measure the accelerating gradient limit of the cavity one should test the cavity at the linear collider working temperature range 1.6 – 2.1K. During the test the cavity is immersed into the liquid helium, which is superfluid at this temperature range. The hot spot on the niobium surface becomes the heat source in the superfluid helium. The heat propagation law in superfluid helium is wavelike and is called second sound [4], [5].

The second sound wave arrival can be detected by oscillating superleak transducers (OST) arranged around the cavity (Fig.2) [6]. The second sound wave velocity is constant for the fixed temperature. Velocity versus temperature experimental curve can be found, for example, in [7], [8]. Let the wave propagate along the straight line. Therefore, the information about the distances between the quench source and the detectors can be obtained and it is sufficient for the heat source location, provided the detectors coordinates are determined and their arrangement does not have symmetry about plane or line.



Figure 2: OST

### 3 Calculation model

We assume the heat source to be a singular hot point in 3d space between the detectors with unknown coordinates. The technique to be created should locate a point in the space, and the distances from it to the detectors should coincide with the measured ones (Fig.4). In fact, we need to find an intersection of several spheres with the centers in each detector (Fig.3). Ideally, all of them would intersect at the same point, so even three detectors would be enough for precise heat source location. But in real experiment there always will be an error present in detectors coordinates, in times measured, and velocity data at given temperature, which will lead to the overall discrepancy, so the spheres intersection will be considered as an area of finite size rather than a point.

The solving method we used is the minimum norm solution: it minimizes the difference between measured distances the signal passes and distances from the detectors to the point suspected to be the hot spot, i.e. it chooses the point in the spheres intersection area from which the total distance to the all spheres surfaces is minimum.

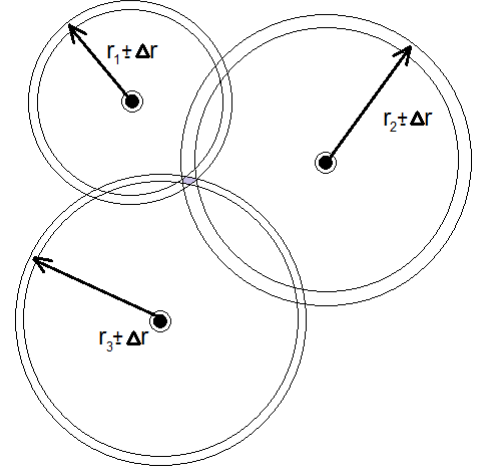


Figure 3: Inverse problem definition

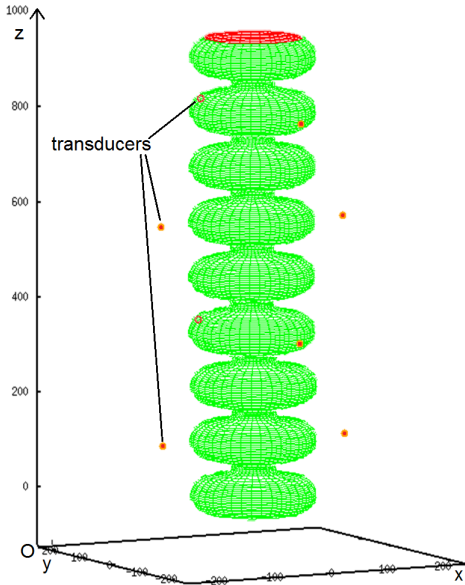


Figure 4: Cavity and transducers plot

Although we assumed the wave path to be the straight line, actually the cavity can shade some detectors against the second sound wave, so it takes longer for the wave to reach them. Thus, the wave path would be some curved line in this case. Concerning the remote detectors, it is possible to a first approximation not to take into account the curved sound wave path error because the error is negligible compared to the distance between this detector and the quench origin. If the transducer is close to the quench origin and in the same time is shaded by the cavity, then we can exclude this transducer result from the calculations.

Thus, we need to solve an overdetermined system of nonlinear equations (1) in terms of minimization:

$$(x_0 - x_i)^2 + (y_0 - y_i)^2 + (z_0 - z_i)^2 = C^2 \cdot t_i^2, \quad i = \overline{1, n} \quad (1)$$

where  $(x_0, y_0, z_0)$  are the quench origin coordinates, i.e. variables;  $(x_i, y_i, z_i)$  and  $t_i$  are respectively coordinates and measured time of the transducer number  $i$ ;  $C$  is the

second sound velocity; and  $n$  is the number of transducers (see Fig.4). To solve it in terms of minimization is virtually to find minimum of the error function  $f(x_0, y_0, z_0)$  (2):

$$f(x_0, y_0, z_0) = \sum_{i=1}^n \left[ (x_0 - x_i)^2 + (y_0 - y_i)^2 + (z_0 - z_i)^2 - C^2 \cdot t_i^2 \right]^2 \quad (2)$$

For minimization we used Nelder-Mead algorithm in GNU Octave implementation (downhill simplex method) [9].

## 4 Output error estimation

The minimum norm solution method defines a point in 3d space with  $(x_0, y_0, z_0)$  coordinates being the heat source. One needs to estimate the accuracy of this result, i.e. determine the most probable distance from this point to the true source on the cavity surface. Detectors position definition makes the greatest contribution to the output error. The wave propagation time can be determined by the second sound transducer with a precision of microseconds, thus the distances can be measured with a precision of  $10^{-4}$ m (the second sound velocity is about 20m/s [7]), whereas the detectors alignment precision at the present point cannot be better than several millimeters. The second sound velocity experimental data being temperature dependent are also accurate within  $10^{-4}$ m/s.

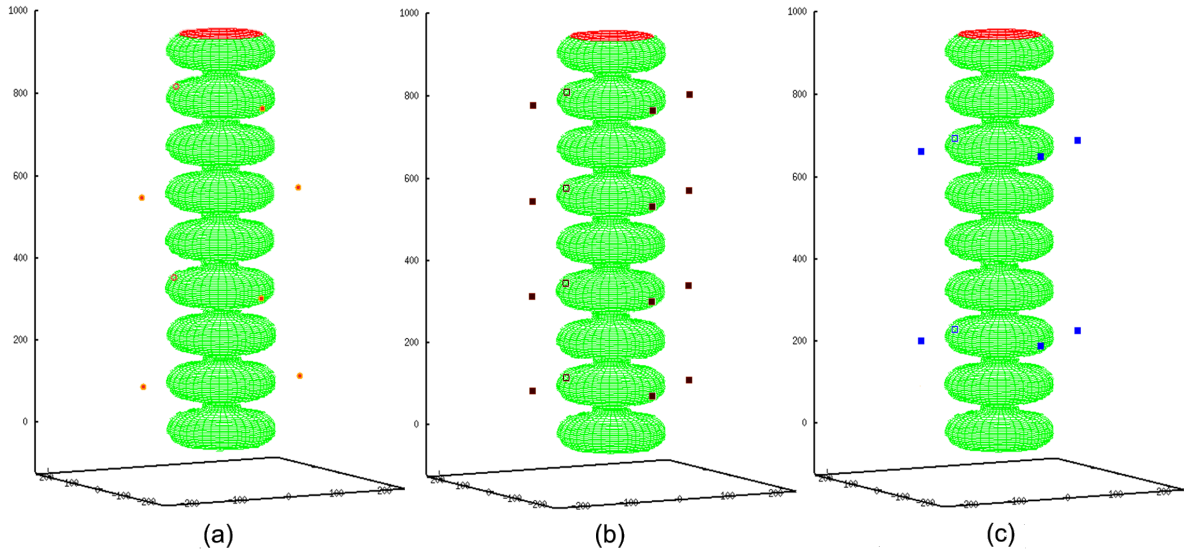


**Figure 5:** Three basic detectors configurations (a) #1, (b) #2, (c) #3

The Monte Carlo simulation method was used to estimate the output error. This method simulates the output result using the artificially created input data with certain RMS deviation. The paths the signal passes are considered the distances between "true" detectors position and quench source locations we choose earlier. After a prolonged iteration the output RMS error is obtained.

We analyzed the output RMS error dependences on the input RMS error for three transducers configurations (see Fig.5). The quench source was supposed to be on the every cell equator of the 1.3GHz 9-cell TESLA cavity, though the developed software allows analyzing any configuration and supposed source points at any time. For each cell the ratio of output error to input error (error gain) appears to be constant in a quite large range of input error (see examples in Fig.6) with slightly different slopes of the output error dependence. Thus, the problem solving technique is stable and convergent.

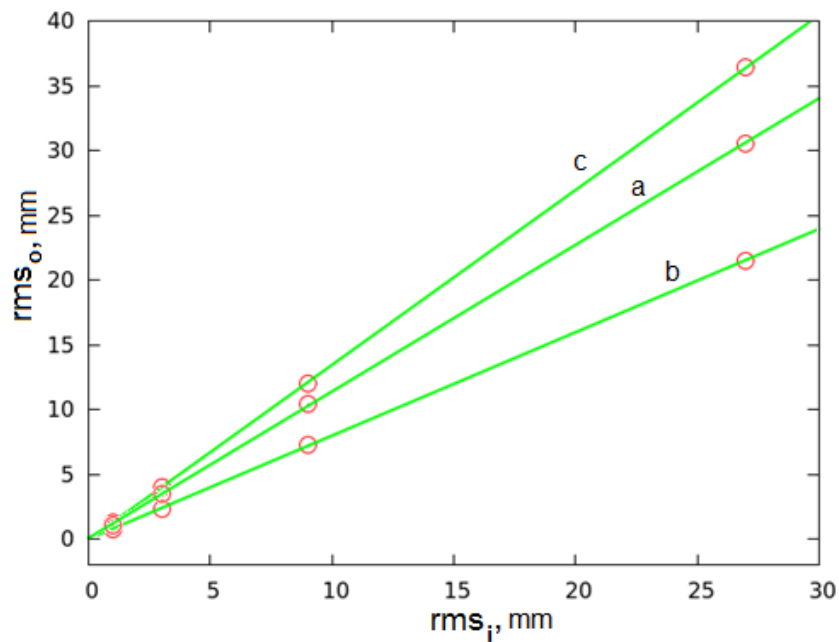


Figure 6: Output error versus input error for configurations (a) #1, (b) #2, (c) #3

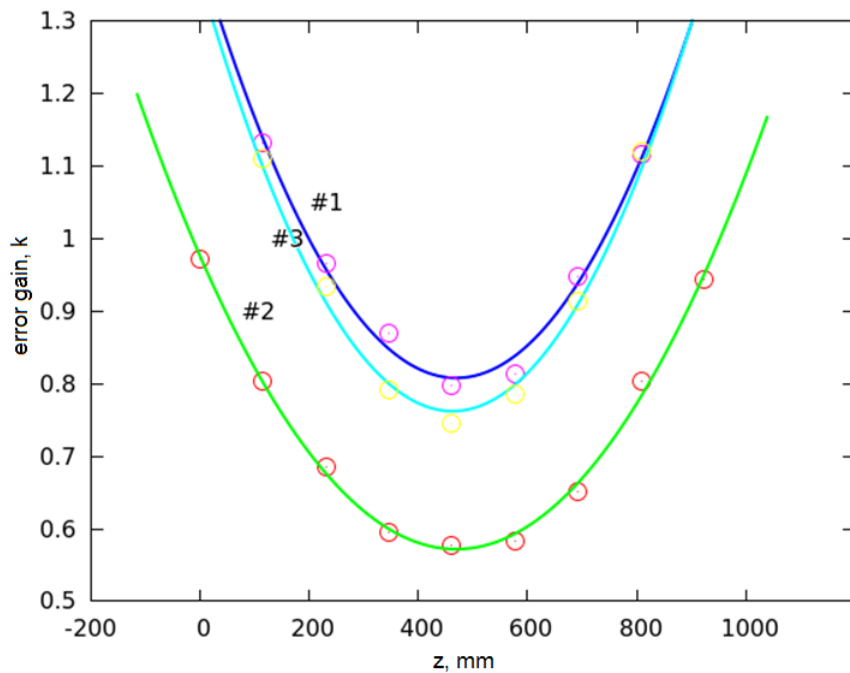


Figure 7: Error gain versus quench z-coordinate for configurations (a) #1, (b) #2, (c) #3

The error gain versus quench origin  $z$ -coordinate curve is necessary for the detectors arrangement optimization. The varying of  $x$  and  $y$  coordinates is not relevant due to the cylindrical symmetry of the cavity. The certain shape of the curve is defined by the detectors configuration. Usually the quench source in the middle cells is more accurately calculated. The simulation results are shown in Fig. 7 for three different configurations (see also Fig.5). Also, it is important to mention that error gain for the method in question can be less than 1. If we double the number of detectors, the error gain significantly decrease (see configuration #2 in Fig.5). Moreover, with 16 transducers the error gain is always less than 1. One should use as much transducers as possible to reduce the output error.

## 5 Cavity surface restriction

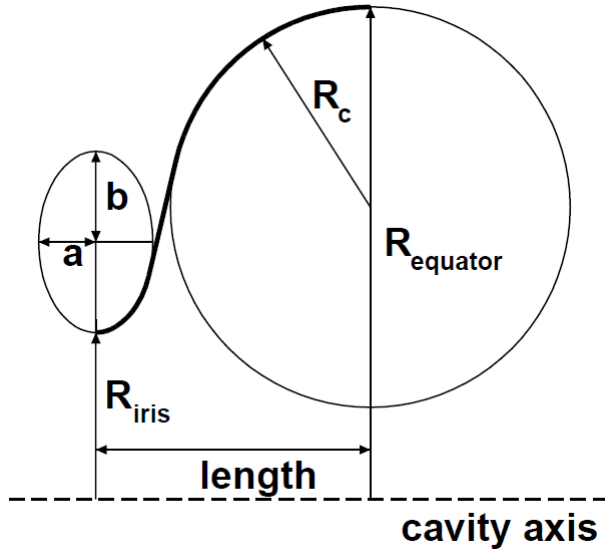


Figure 8: SRF TESLA cavity longitudinal crosssection

Up to now the problem solving did not take into account the cavity by any means: it was only detectors coordinates in some frame of reference that were relevant.

The output of the calculations is the point coordinates in the same frame of axis. So, this technique can be used for quench location on the surface of any shape cavity. To link the result to the cavity per se one needs to determine the position of the cavity symmetry axis. But, if the cavity surface can be

modeled, it is possible to reduce the resulting RMS error by restricting the heat source location to the surface, because it is obvious that the quench can appear only on the cavity surface. In fact, three-dimensional space of variables reduces to the two-dimensional manifold. Thus, the presented technique searches for the minimum point of the error function only among the points on the cavity surface.

We used 9-cell and single-cell SRF TESLA cavities in the experiments. Its longitudinal section is shown in Fig.8 with parameters from Table 1 [1]. Its 3d model was developed and the result was plotted in the gnuplot software (see Fig.4). Let  $x$ ,  $y$ , and  $z$  coordinates be functions of two new variables  $z'$  and  $\alpha$ , where  $z = z'$  and  $\alpha$  is the angle in the  $xOy$  plane ( $y = R(z) \cdot \sin \alpha$ ,  $x = R(z) \cdot \cos \alpha$ ,  $R(z)$  is the cavity radius);  $Oz$  is the detectors symmetry axis. Two variables are enough for describing the working coordinate space: the point on the cavity surface is unambiguously defined by its  $z$ -coordinate and angle in the previous coordinate system  $xOy$  plane. Then the minimizing function  $f$  will take the following form:

**Table 1:** Half-cell shape parameters

Cavity shape parameter (mm)	Midcup	Endcup 1	Endcup 2
Equator radius $R_{equator}$	103.3	103.3	103.3
Iris radius $R_{iris}$	35	39	39
Radius of circular arc $R_c$	42.0	40.3	42
Horizontal half axis $a$	12	10	9
Vertical half axis $b$	19	13.5	12.8
Length $l$	57.7	56.0	57.0

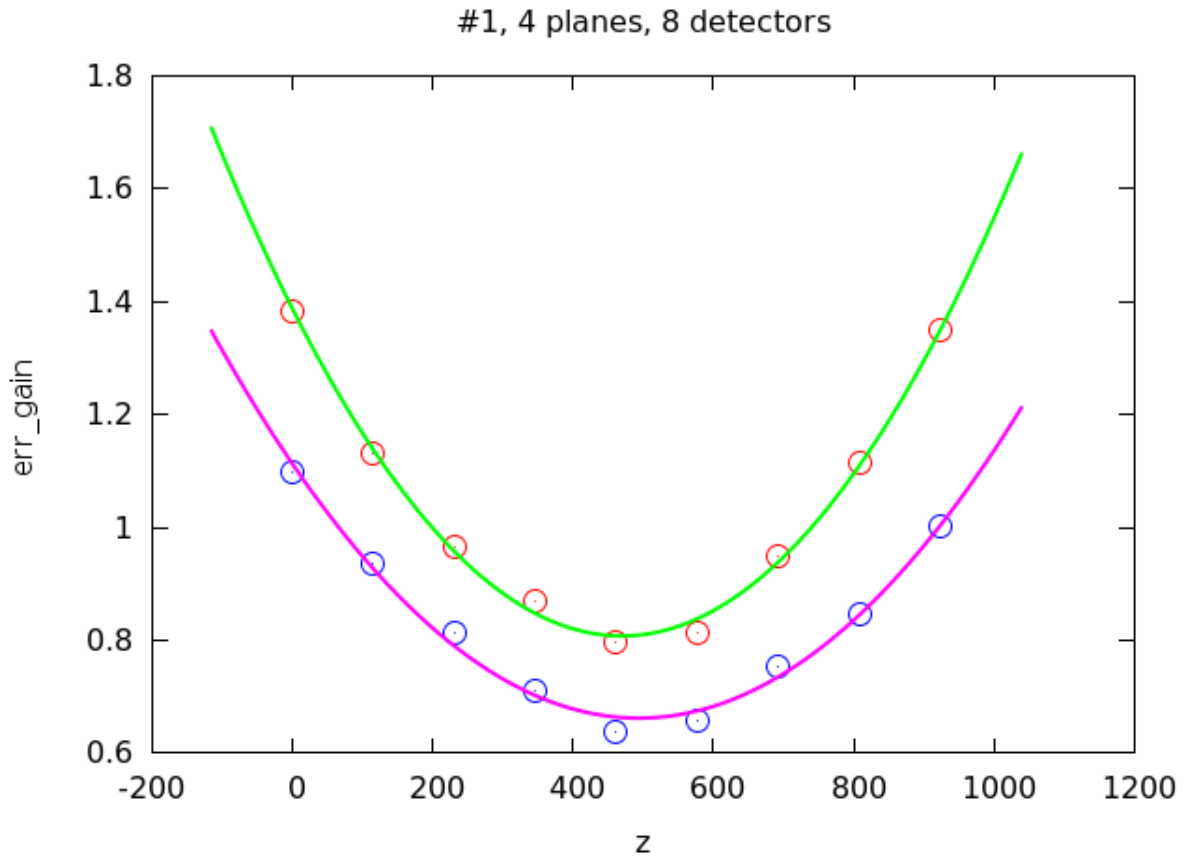


**Figure 9:** Error gain versus quench  $z$ -coordinate for configuration #1

$$f(\alpha_0, z'_0) = \sum_{i=1}^n \left[ (x_0(\alpha, z'_0) - x_i)^2 + (y_0(\alpha, z'_0) - y_i)^2 + (z'_0 - z_i)^2 - C^2 \cdot t_i^2 \right]^2 \quad (3)$$

Thus, we made sure the result to be on the cavity surface. The error gain versus z-axis curves for cavity-independent and cavity-dependent cases are shown in Fig.9. The error gain decreased even more, providing a greater improvement of accuracy. However, there is always a prospect of a mistake made somewhere in calculation. For example, the result could appear between the cells, so one could conclude the possibility of some incorrect input data, but with the cavity surface restriction it would pass unnoticed because the point would be definitely projected to the surface. So, both techniques are essential for fail-safe, consistent, and accurate result.

## 6 Data collection

### 6.1 Experimental procedure

All the experiments were done in the Vertical Test System (VTS 1). The cryostat can hold up to 1000 liters of superfluid helium and has cooling power of about 200W at 2.0K and about 100W at 1.8K. RF testing in VTS is performed in continuous wave (CW) mode: the rf power ( 100W) at resonance frequency (1.3GHz ) is applied to the cavity through a weakly-coupled antenna. It takes few seconds for the rf-field inside the cavity to reach the critical amplitude. Once this happens, the cavity quenches. Then the process repeats in pseudo-periodic fashion again and again.

The OSTs are essentially capacitive "microphones" (see Fig.2) with capacity  $C_{OST} \simeq 50pF$ . We used a DC-bias scheme to read them out (Fig.10).  $C_{in}$  is approximately 100nF. The preamp is located on the top of the cryostat in an attempt to reduce the length of the parasitic capacitance of the cable ( $C_x \sim 500pF$ ) to the OST. The amplified signal was routed to the instrumentation rack where it was read by 24-bit data-acquisition (DAQ, NI 9239) electronics. The same DAQ read all 8 OST channels as well as the transmitted rf-power and vapor pressure in the helium dewar. The complete scheme can be found in appendix (see Fig.19).

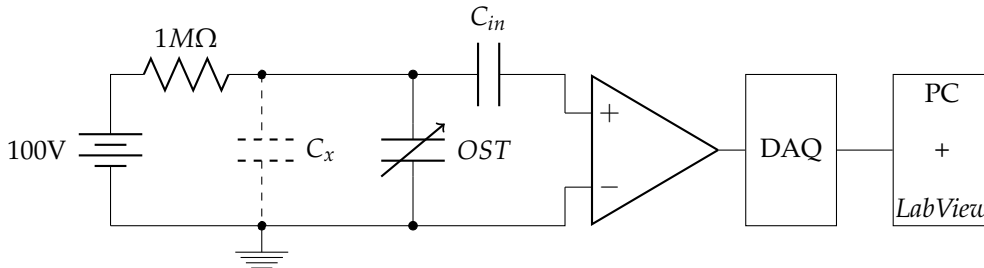
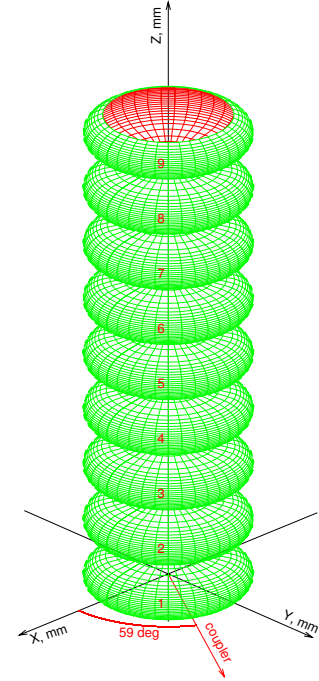


Figure 10: OST reading out scheme

## 6.2 Input data

### 6.2.1 Detectors coordinates

Our coordinate system and its relation to so-called "Kyoto coordinate system"[10] are shown in Fig.11. In the last one the point on the cavity surface is defined by (a) number of the cell, (b) distance to the weld along the surface, and (c) angle in degrees counterclockwise from the coupler direction in the plane perpendicular to the cavity symmetry axis. We choose this system so that several transducers are located in either  $xOz$  or  $yOz$  planes for 9-cell cavity experiments. In the developed software several most frequent configurations are already calculated (for example, the three configurations in Fig.5). One can use the given configurations or add to the function text a new one.



**Figure 11:** The current (black) and Kyoto (red) coordinate systems

### 6.2.2 Time readings

*LabVIEW* software records output of the OST simultaneously with the amplitude of transmitted RF-power and the helium vapor pressure in the bath. The transmitted power indicates the onset of the quench. The vapor pressure could be used to find an equilibrium temperature of the bath.

Due to a high bandwidth requirement the data were streamed to disk in *LabVIEW*-specific TDMS binary format. The data could be converted into ASCII offline by another *LabVIEW* program. The developed Octave script processes the file and created the group of files with  $(t, y(t))$  columns for every time-dependent value, which can be easily plotted in Octave or gnuplot. Then these files should be processed manually.

Although the moment of time when the second sound wave reaches the transducer surface can be precisely determined from these data, usually it is not obvious which peak is related to the second sound wave. The example of the detectors readings is shown in Fig.12. However, provided the cavity quenches in the same spot, the detectors data reproduces itself each time with high precision. So, the tiny peaks are not the noise but the first sound wave itself, first sound reflections, second sound reflections, etc. Usually the second sound peak is the highest one and can be easily identified (see channels 1, 2, 3 in Fig.12, but sometimes it is ambiguous (like on channels 4, 5), especially for the remote detectors. The ultimate goal is to computerize the whole second sound quench detection and to integrate the software into the existing system that deals with the experiment. The ambiguity of the time interval reading

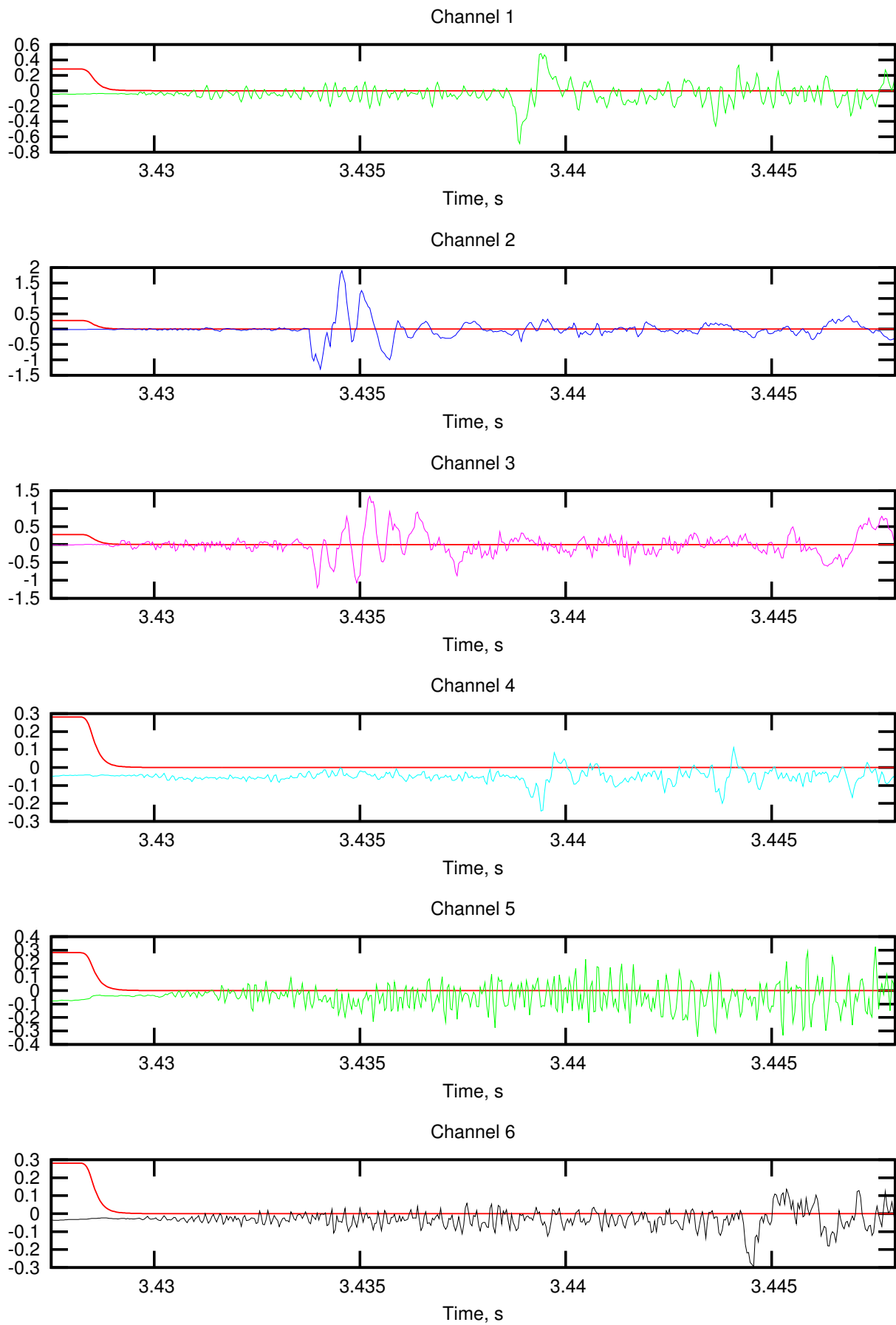


**Figure 12:** Second sound transducers readings

is one of the main obstacles to that goal. Now, when it is impossible to discriminate several peaks in the plot, one can either exclude this detector from the calculations, decreasing thereby the ultimate accuracy, or try to use different time data for one detector in the calculations. One should save the time readings in the file in a form of a column: first is the quench time determined by the RF system; next is the wave arrival times, determined by each detector, one after another according to their sequence number.

### 6.2.3 Second sound velocity

The second sound velocity can be determined from the velocity versus temperature experimental curves [8], [7]. The temperature depends on the helium pressure, which is approximately constant during one-quench test. The *LabVIEW* file processing script calculates the working temperature and saves it to another file.

## 6.3 Data analysis

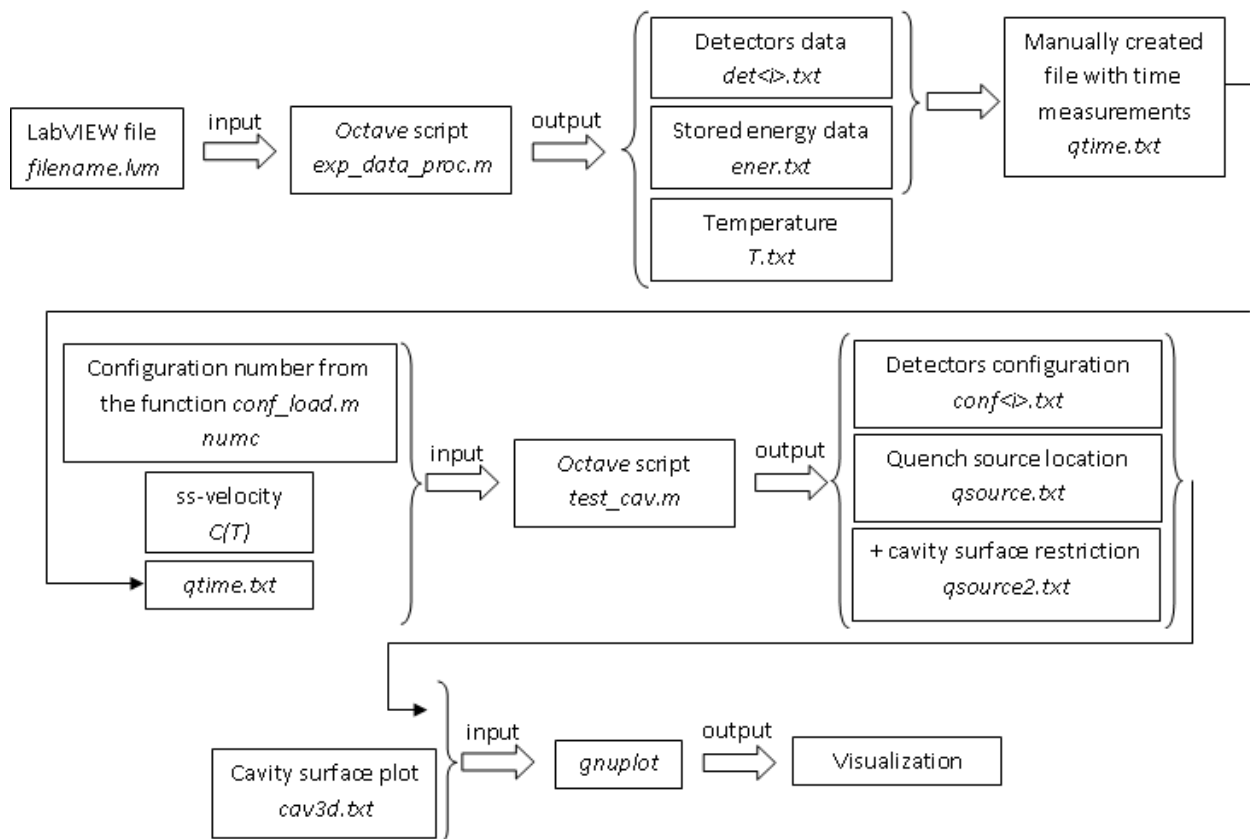


Figure 13: User manual

One should launch the developed software for the current detectors configuration, the time readings taken, and the second sound velocity for the temperature during the test, and obtain the quench origin coordinates, which will be saved to the file. The second result will be obtained by using the cavity surface restriction and also saved to the file. The complete manual is on the scheme in Fig.13.

We used gnuplot software for visualizing the result. All the coordinates should be in the same frame of axis, which is chosen before the test. Thus, one can find out the quench source location relative to the detectors and the cavity in 3d space. The simple, geometry based program then can transform the result to the Kyoto coordinate system: angle in degrees, number of the cell and the distance from the weld (see Fig.11).

## 7 Experimental results

### 7.1 Quench location examples

#### 7.1.1 single-cell te1acc06

16 thermometers were attached equidistantly on the weld of the cell. None of them show a clear quench signal. Analysis of the 2nd-sound data indicates that the quench origin was several centimeters lower than the weld with accuracy about half a centimeter (Fig.14 (a)). We explored the inner surface of the cavity with the Fermilab cavity Optical Inspection System and found a typical cat-eye defect in the location determined by the software to be the quench source (Fig.14 (b)). Since there were not any defects in the neighborhood, one can assume that we succeeded in locating the quench origin in this experiment.

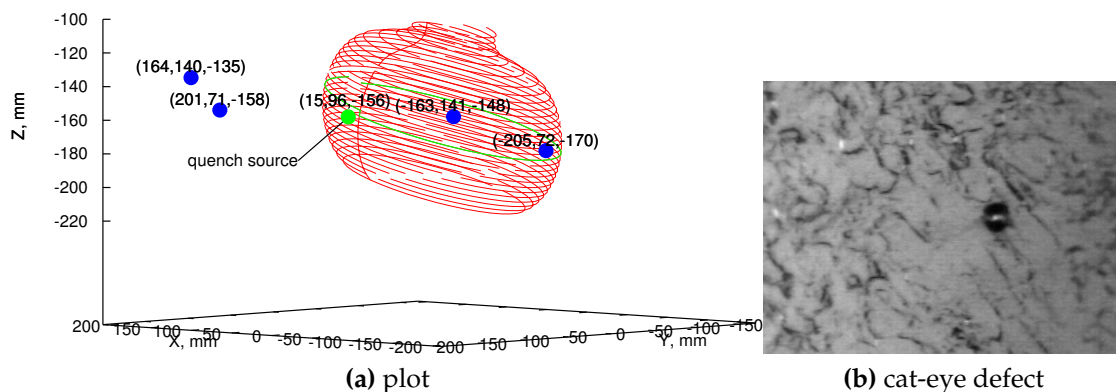


Figure 14: te1acc006

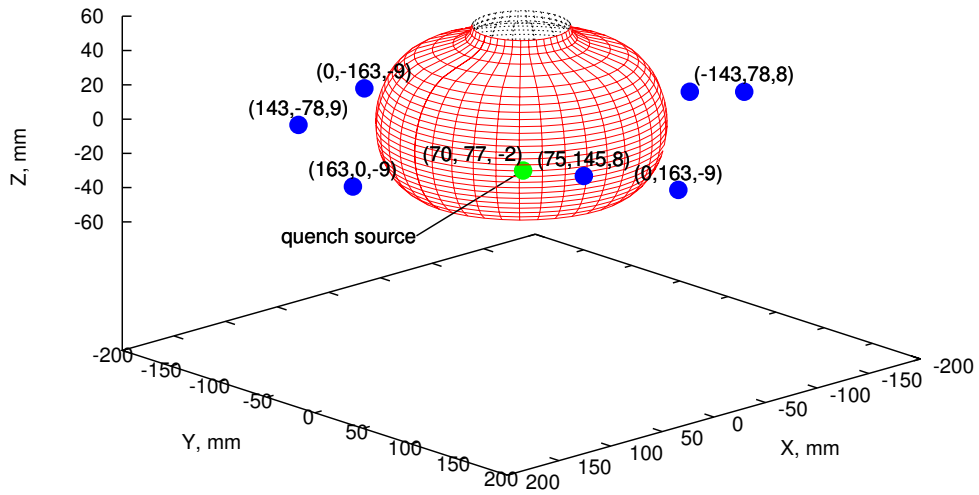


Figure 15: telacc005

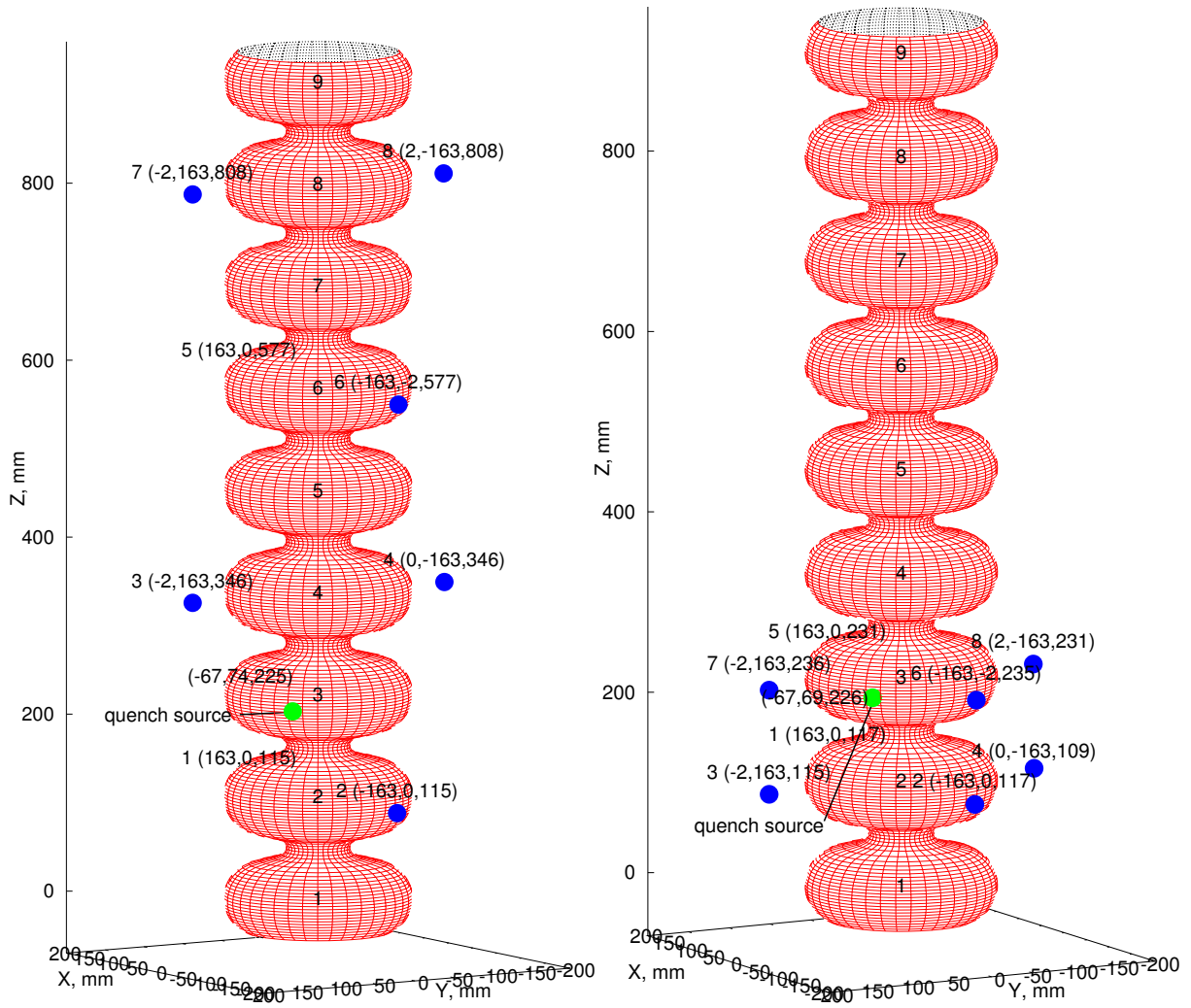


Figure 16: tb9aes003

### 7.1.2 single-cell te1acc005

Quench was located on the weld of the cavity as it shown in Fig.15, and thermometry confirmed this result.

### 7.1.3 9-cell tb9aes003

This cavity is the only one which was tested two times successively with different detectors configurations. The quench was located in the same place with an error less then 5 mm. The results are shown in Fig.16(a) and (b) . Fast thermometry confirmed the result obtained.

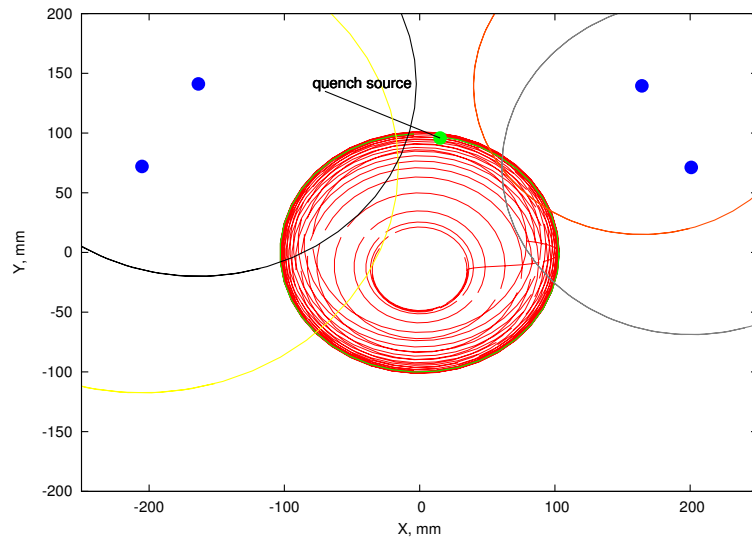
## 7.2 Time readings inconsistency

The experiments revealed a considerable discrepancy in the time readings: almost all of the transducers provided the time readings with at least 30% shortage of second sound propagation time. The signal propagation spheres should intersect in a small area the size of at least a  $\text{cm}^2$ . In example in Fig.17 one can see that some of the spheres do not intersect at all. This result was obtained in several experiments with both 9-cell and single-sell cavities. The cavities we discussed earlier and several transducers with their signal propagation spheres in  $xOy$  projection for cingle-cell and in vertical projection for 9-cell cavities are shown in Fig.17.

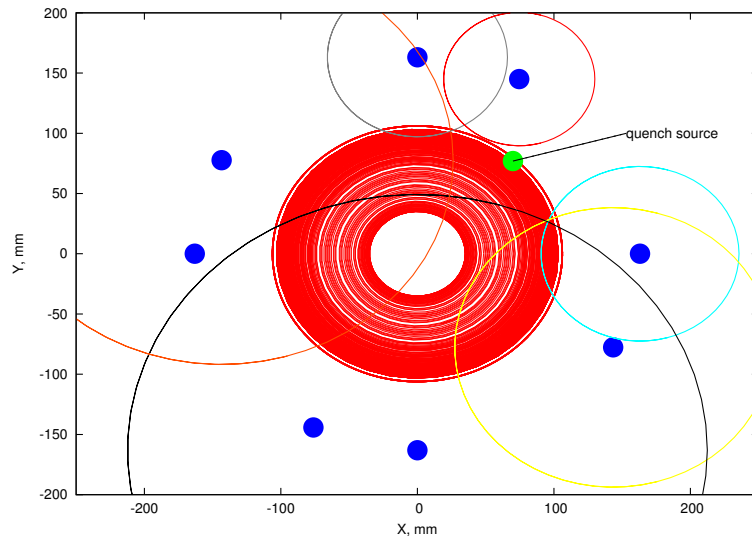
The readings of the transducers facing the cavity is shown in Fig.18. It is easy to see that the gap is present between the transducers propagation spheres and the cavity surface, but it is relatively small and about 7% of the measured distance, whereas other transducers showed almost constant and more considerable distance shortage about 5 cm (see example in Table 2). Strictly speaking, the exact value and its deviation depends on the specific detectors configuration.

**Table 2:** Time readings for tb9aes003 cavity,  $C \simeq 19.95$  m/s

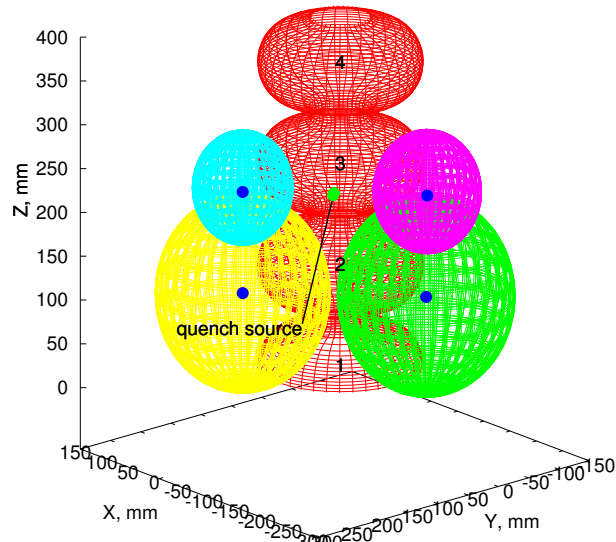
Transducer number	Time shortage, ms	Distance shortage, mm
1	2.5223	50.32
2	2.6081	52.03
3	2.6871	53.61
4	2.6173	52.21
6	2.5327	50.53



(a) te1acc006



(b) te1acc005



(c) tb9aes003

Figure 17: Time readings deficiency

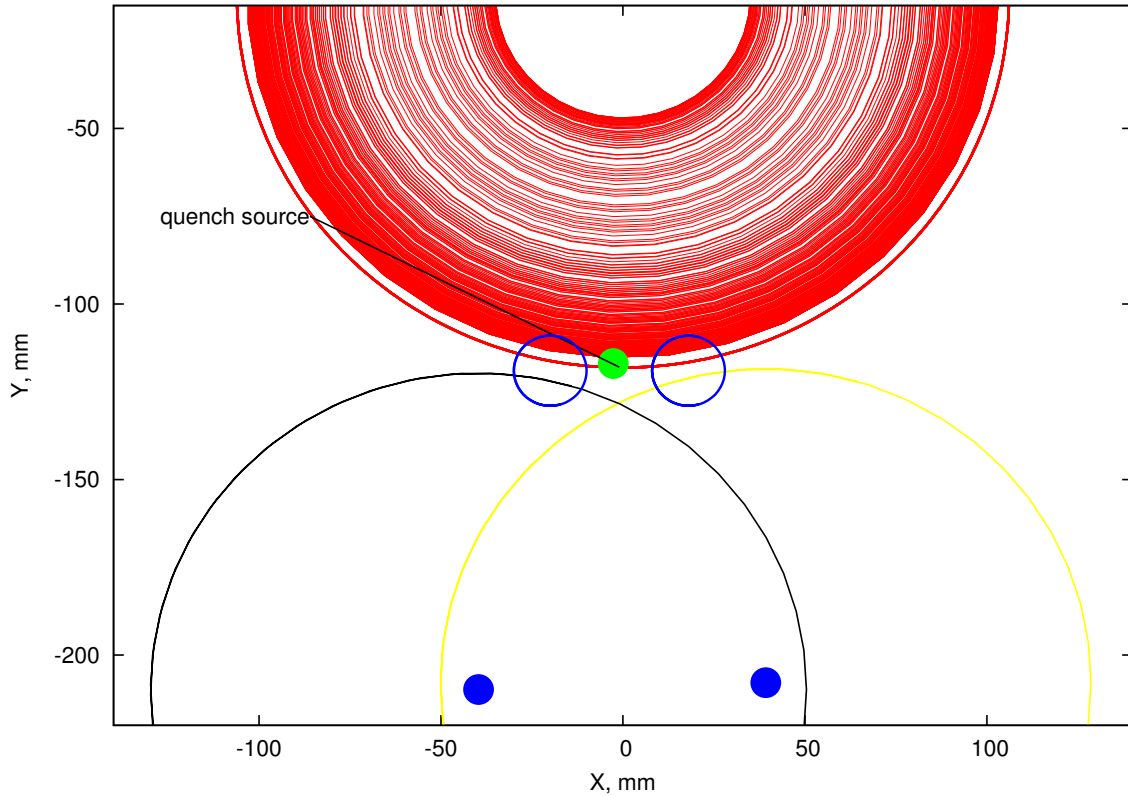


**Figure 18:** Shortage of second sound propagation time for the transducers facing the cavity

### 7.3 Possible explanations

The model we used in the calculations had an underlying assumption that the source was point-like. However, one cannot locate a singular hot spot on the cavity surface using obtained time readings: the experimental time data are at least 10% less than theoretically predicted ones. In the performed experiments there was no possibility for the time readings random error to be more than 0.2% of the time measurement. Thus, a quench model should incorporate the finite size of the heat source.

In Fig.17 (a) two spheres and the cavity surface intersect in one point with an accuracy of a millimeter. The same is true for two other detectors. One can observe the similar result in Fig.17 (b) and (c). This is consistent with a hot-spot diameter of approximately several centimeters.

The quench locating software was used for two groups of detectors to locate the edges of the hot spot. The diameter of the spot was found to be approximately 8 cm for several cavities including the ones mentioned above. This result could be an experimental proof of the finite size heat source. It is important to mention that the second sound wave is quite slow ( $C = 20\text{m/s}$ ), so the hot spot on the cavity surface appears almost immediately compared to the time of heat propagation in superfluid helium, and the detectors receive initially the signal from the closest points of the hot spot.

The time reading discrepancy for detectors facing the quench origin cannot be

explained with a surface hot spot model. Thus, one more conclusion regarding the quench process is that there is a three-dimensional heat source rather than a two-dimensional. It can be drawn from the Fig.18. We put forward an explanation that there is a helium blob around the hot surface, or the numerous hot helium bubbles, which propagates the heat wave itself and appears in some point faster than the second sound wave from the niobium reaches the same point. The temperature of the hot spot, measured by the thermometer, can reach 100K, so helium must be boiling around the quench epicenter. The size of the area, containing gaseous helium, appears to be 2-3 millimeters approximately due to the simple analysis of the measured distance discrepancy. This distance appears to be relatively small compared to the large size of the hot spot. Moreover, it arises only in the detectors facing the quench source. Thus, at this stage helium bubble error can be neglected.

## 8 Summary

The method seems to produce a relatively good result despite the time readings discrepancy. For the remote detectors the hot spot error is approximately constant, and for the error function minimum point the constant time addition makes no difference. Though, the error will be higher than it was predicted by Monte Carlo simulation.

Therefore, the next approximation after a point source is a circular symmetrical source on the cavity surface. At this stage we can calculate the hot source edge points using selected transducers, but this requires thorough analysis and reduces the accuracy due to decreased number of ss-transducers, though the result is still acceptable. Thus, we need to estimate the actual physical properties of the hot spot on the surface and embed them in our model in order to produce an accurate result.

The time-dependent analysis of the quench process can also be helpful. It is still obscure what the temperature dependence on time and distance is and how it could influence the second sound wave propagation times.

## 9 Conclusion

In this paper we presented the technique of quench location with the second sound wave in superfluid helium. The method works and experimental results are satisfactory despite the discovered discrepancy for the second sound wave propagation times. By analyzing the data we found that the approximation where the 2nd-sound emitter is a near-singular source does not describe the physical system well enough. Thorough analysis of the quench process physics can be helpful in creating a more adequate model.

## 10 Acknowledgment

This work was performed in part during internship with Fermilab's PARTI program under supervision of Dr. D.A.Sergatskov.

## References

- [1] B. Aune and etc. Superconducting tesla cavities. *Physical Review Special Topics - Accelerators and Beams*, 3(2), 2000. 2, 6
- [2] J. Knobloch. *Advanced Thermometry Studies of Superconducting Radio-Frequency Cavities*. PhD thesis, Cornell University, 1997. 2
- [3] G. Ciovati. *Investigation of the Superconducting Properties of Niobium Radio-Frequency Cavities*. PhD thesis, Old Dominion University, 2005. 2
- [4] I.M. Khalatnikov. *An Introduction to the Theory of Superfluidity*, volume 49. "Nauka", Moscow, 1965. 2
- [5] C. Enns and S. Hunklinger. *Low-Temperature Physics*. Springer, 2005. 2
- [6] R. A. Sherlock and D. O. Edwards. Oscillating supedeak second sound transducers. *The Review of Scientific Instruments*, 41, number 11, 1970. 2
- [7] D. Greywall and G. Ahlers. Second-sound velocity, scaling, and universality in he ii under pressure near the superfluid transition. *Physical Review Letters*, 28, number 19(3), 1972. 2, 4, 11
- [8] R. Donnelly and C. Barenghi. *The Observed Properties of Liquid Helium at the Saturated Vapor Pressure*, volume 14. 1977. 2, 11
- [9] G. Borse. *Numerical Methods with MATLAB«: A Resource for Engineers and Scientists*, volume 3. PWS Pub. Co., 1996. 4
- [10] Y. Iwashita. Tesla technology collaboration meeting. DESY, 2008. 9

# A Appendix

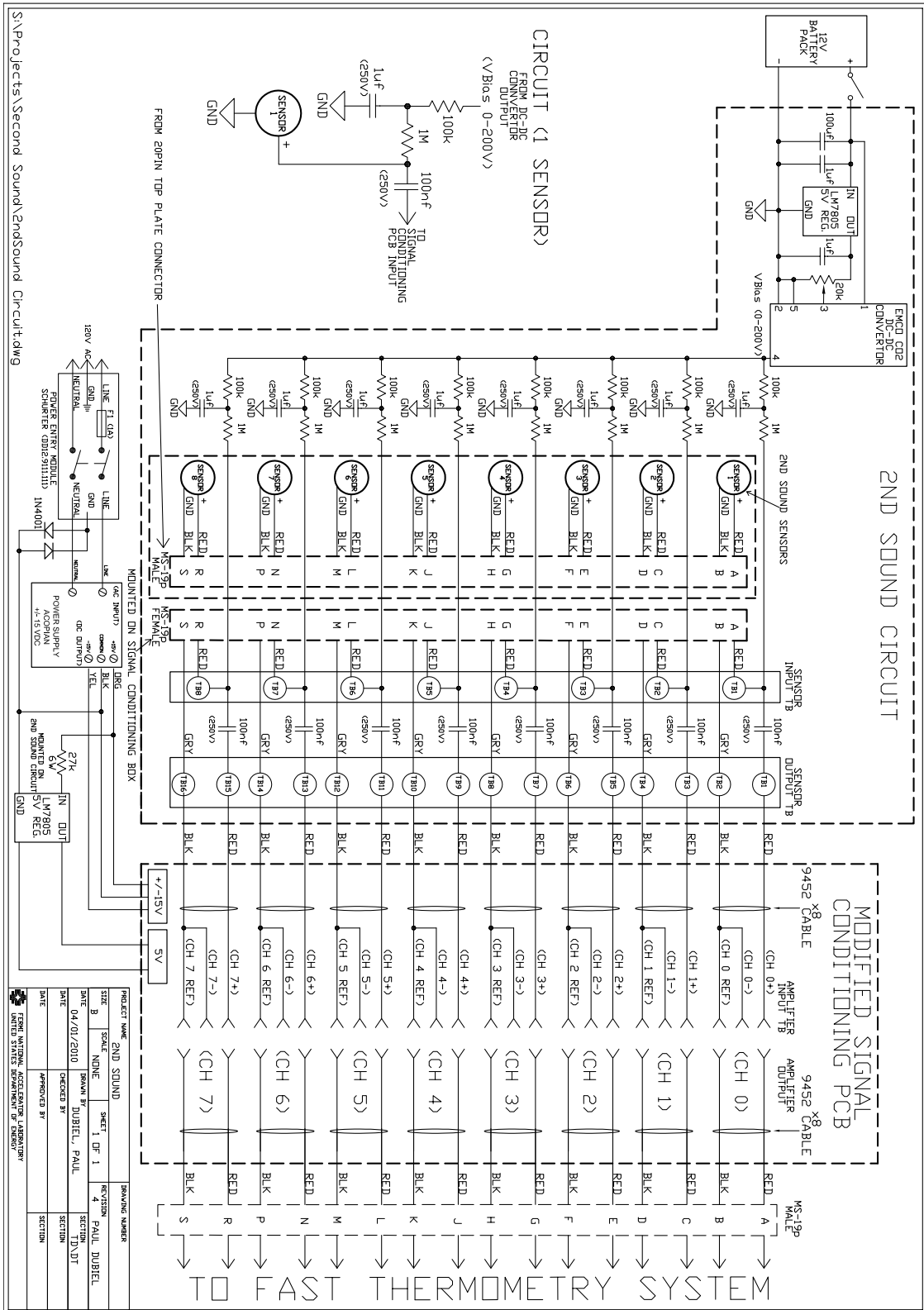


Figure 19: Second sound experiment circuit